ELSEVIER

Journal of Alloys and Compounds 388 (2005) 284–292

Journal of ALLOYS AND COMPOUNDS

www.elsevier.com/locate/jallcom

Effects of substituting Co with Fe on the microstructures and electrochemical characteristics of the as-cast and quenched $Mm(NiMnSiAl)_{4.3}Co_{0.6-x}Fe_x$ (x = 0–0.6) electrode alloys

Yan-ping Zhao[a], Yang-huan Zhang[b,c,*], Guo-qing Wang[c], Xiao-ping Dong[c], Shi-hai Guo[b], Xin-lin Wang[b]

[a] *Department of Material, Tianjin Institute of Technology, Tianjin 300191, China*
[b] *Department of Functional Material Research, Central Iron and Steel Research Institute, Beijing 100081,China*
[c] *School of Material, Inner Mongolia University of Science and Technology, Baotou 014010, China*

Received 19 April 2004; received in revised form 26 July 2004; accepted 26 July 2004

Abstract

The microstructures of the rare-earth-based AB_5-type $Mm(NiMnSiAl)_{4.3}Co_{0.6-x}Fe_x$ (x = 0, 0.1, 0.2, 0.3, 0.4, 0.5, and 0.6) hydrogen storage alloys were analysed by XRD, SEM and TEM, and electrochemical characteristics of the as-cast and quenched alloys were measured. The effects of substituting Co with Fe on microstructures and electrochemical characteristics of the as-cast and quenched alloys were investigated in detail. The obtained results show that the effects of substituting Co with Fe on the phase structures of the as-cast and quenched alloys are imperceptible, but its effects on electrochemical characteristics of the alloys are notable. The discharge capacities decrease, but the cycle lives of the alloys were improved with the increase of the amount of Fe substitution. Especially, substituting Co with Fe can significantly enhance the cycle lives of the as-quenched alloys, which is mainly attributed to the grain refinement caused by substituting Co with Fe.

Keywords: Substituting Co with Fe; As-cast and rapidly quenched; AB_5-type hydrogen storage alloy; Microstructure; Electrochemical characteristics

1. Introduction

Since the commercialization of small size Ni-MH cells in 1990, it has gained a good share in the severe competition of the rechargeable battery market for several years. The application prospect of Ni-MH cells attracted researchers' interest all over the world. In the very recent years, however, the rechargeable Ni-MH cells are facing serious challenge owing to quick development of Li-ion cells. On the one hand, the Li-ion cells show higher energy density than the Ni-MH cells per unit weight or volume. On the other hand, the production cost of Ni-MH battery-based on the current technology also limits its widespread applications because low-cost Pb-acid batteries are still dominating the sector. Thus, the electrochemical performance enhancement and the cost reduction of the hydrogen storage alloy are extremely critical to competition. The studies of the positive electrode of Ni-MH battery have already attained high level, and its capacity nearly approached to theoretical one. For the negative materials, the electrochemical capacity of current advanced AB_5-type alloys has reached 310–330 mAh/g. Therefore, further improvement on the capacity of AB_5-type alloys seems to be difficult since the theoretical capacity of $LaNi_5$ is about 372 mAh/g. In order to broaden application field of Ni-MH batteries and enhance their competition abilities, a realistic approach is to reduce the production cost of hydrogen storage alloy. According to the typical AB_5-type alloy formula, e.g. $MmNi_{3.5}Co_{0.75}Mn_{0.4}Al_{0.3}$, Co content takes up about 10 wt.% and 40–50% share of the total cost of the raw materials, and the price of Co is increasingly going up in international market. Due to Co reserves, it is unrealistic to expect the great slump of Co price. Thus, researchers have

* Corresponding author. Tel.: +86-10-62187570; fax: +86-10-62182296.
E-mail addresses: zyh59@yahoo.com.cn, ljlgrace@vip.sina.com (Y.-h. Zhang).

0925-8388/$ – see front matter © 2004 Elsevier B.V. All rights reserved.
doi:10.1016/j.jallcom.2004.07.020

naturally paid much attention on the decrease of Co content in the alloys [1–9]. Although researchers have done much work in preparing low-Co and Co-free hydrogen storage alloys around the world, the obtained results are still unsatisfactory [4–7]. The main problem is that the cycle stabilities of low-Co and Co-free AB_5-type electrode alloys are very poor because the function of Co on the cycle stability of AB_5-type hydrogen storage alloy is extremely important [10]. In order to improve the cycle stabilities of low-Co and Co-free hydrogen storage alloys, multi-component AB_5-type hydrogen storage alloy with single phase or two-phase structure have been prepared by rapid quenching in our previous research [1–3], and investigation results show that low-Co and Co-free AB_5-type hydrogen storage alloys with high capacity and long cycle life can be prepared by scientific composition design and using rapid quenching technique. The paper studied the effects of substituting Co with Fe on the microstructures and electrochemical characteristics of the as-cast and quenched $Mm(NiMnSiAl)_{4.3}Co_{0.6-x}Fe_x$ (x = 0, 0.1, 0.2, 0.3, 0.4, 0.5, and 0.6) electrode alloys, and obtained some important results.

2. Experimental

2.1. Alloy preparation

The chemical compositions of the experimental alloys are $Mm(NiMnSiAl)_{4.3}Co_{0.6-x}Fe_x$ (x = 0, 0.1, 0.2, 0.3, 0.4, 0.5, and 0.6). Corresponding with Fe content x, the alloys are represented with Fe_0, Fe_1, Fe_2, Fe_3, Fe_4, Fe_5, and Fe_6. The purity of all the component metals (Ni, Mn, Co, Si, Al, and Fe) is at least 99.7% Mm denotes Ce-rich Mischmetal (23.70 wt.%La, 55.29 wt.%Ce, 5.31 wt.%Pr, and 15.70 wt.%Nd) with the purity of 99.85 wt.%. The alloys were melted in an induction furnace in an argon atmosphere and cooled in a water-cooling copper mould, and the parts of the as-cast alloys were remelted and quenched by melt-spinning with a rotating copper wheel, obtaining flakes of the as-quenched alloy with quenching rates of 10, 16, 22 and 28 m/s. The quenching rate is expressed by the linear velocity of the copper wheel.

2.2. Microstructure determination and morphology observation

The samples of the as-cast alloys were directly polished and flakes of the as-quenched alloys were inlaid in epoxy resin for polishing. The samples, thus prepared, were etched with a 60% HF solution. The morphologies of the as-cast and quenched alloys were observed by SEM. The samples of the as-cast and quenched alloys were pulverized by mechanical grinding, getting the power samples with the size less than 50 μm. The phase structures and lattice parameters of the as-cast and quenched alloys were determined by X-ray diffractometer of D/max/2400. The diffraction was performed with $CuK_{\alpha 1}$ and the rays were filtered by graphite. The experimental parameters for determining phase structure are 160 mA, 40 kV and 10 °/min, respectively. The powder samples were dispersed in absolute alcohol for observing the grain morphology with TEM. The granular morphologies and the chemical component change of the surface of alloy electrode before and after electrochemical cycle were observed and analyzed by SEM in order to reveal the mechanism of the efficiency loss of the alloy electrode.

2.3. Electrode preparation and electrochemical measurement

The parts of the as-cast and quenched alloys were mechanically ground into powder below 250 mesh. Electrode pellets (d = 15 mm) were prepared by mixing 1 g alloy powder and 1 g Ni powder as well as a small amount of polyvinyl alcohol (PVA), and then compressed under a pressure of 35 MPa for 5 min. After drying for 4 h, the electrode pellets were immersed in KOH (6 M) solution for 24 h in order to wet fully the electrodes before the electrochemical measurement. The electrode pellet was fixed on the outgoing line of a negative electrode of an open tri-electrode cell and the electrochemical characteristics were measured. $Ni(OH)_2$/NiOOH was the positive electrode of the experimental cell, Hg/HgO the reference electrode and 6 M KOH solution the electrolyte. The voltage between the negative electrode and the reference electrode was defined as the discharge voltage. Every cycle was overcharged to about 30% with constant current, resting for 15 min and −0.500 V cut-off voltage. The activation performance and the maximum discharge capacity were measured with a current density of 60 mA/g, and the cycle life with a current density of 300 mA/g. The environmental temperature of the measurement was kept at 30 °C.

3. Results and discussion

3.1. Microstructure

3.1.1. Phase composition and structure

The phase composition and structure of the as-cast and quenched alloys were determined by XRD. The X-ray diffraction diagrams of the electrode alloys were illustrated in Fig. 1. It can be seen from Fig. 1 that the as-cast alloys have a two-phase structure composed of a $CaCu_5$-type main phase and a small amount of Ce_2Ni_7-type secondary phase. The effect of substituting Co with Fe on the two-phase structures is not obvious. After the alloys are quenched with quenching rate of 22 m/s, the amount of Ce_2Ni_7 secondary phase decreases and the diffraction peak intensity of the (0 0 2) crystal plane increases notably. It can be seen from Fig. 1(b) that the intensities of the diffraction peaks of the as-quenched alloys with different composition are basically uniform. This shows that the crystalline orientation of the as-quenched alloys is more homogeneous. The lattice constants of the as-cast and quenched alloys were calculated from the diffraction peaks

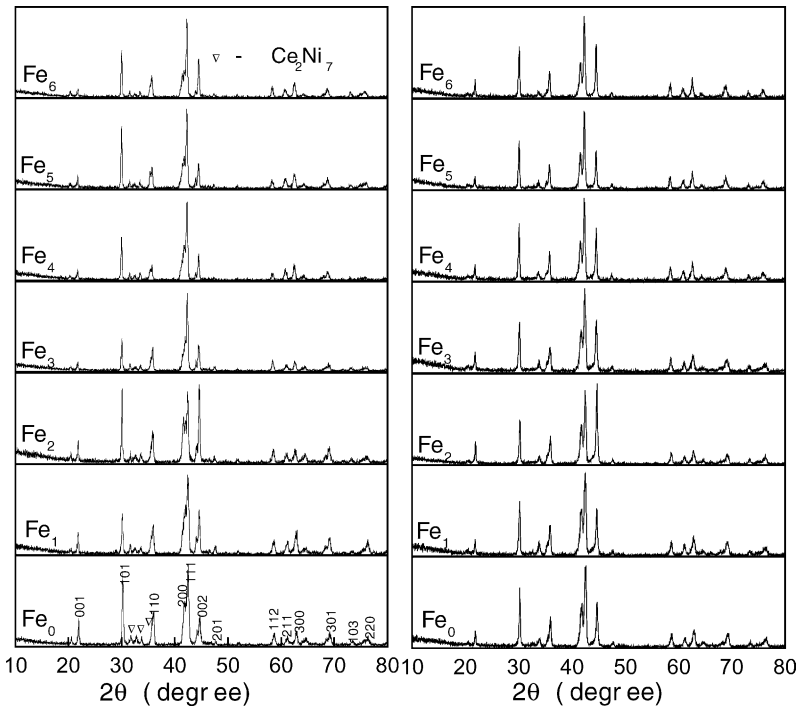

Fig. 1. The X-ray diffraction patterns of the as-cast and quenched alloys (a) as-cast (b) as-quenched (22 m/s).

of (1 0 1), (1 1 0), (2 0 0), (1 1 1) and (0 0 2) crystal planes of the main phase of the alloys by a method of least squares and cell volumes of the alloys were calculated with formula $V = a^2 c \sin 60^\circ$. The calculated results were listed in Table 1. It can be derived from Table 1 that the lattice constants and cell volumes of the alloys slightly increased with the increase of the Fe content, but several exceptions exist among the experimental results. This shows that the compositions of different part of as-cast alloy ingot have a large deviation from the nominal composition of the alloy.

3.1.2. Microstructure morphology

The microstructure morphologies of the as-cast alloys were observed by SEM, and the results were illustrated in Fig. 2. Fig. 2 shows that the grain sizes of the as-cast alloys are very large and the composition homogeneity of the as-cast alloys is very poor. The results of micro-zone energy spectrum analysis with SEM, which were listed in Table 2, show that the as-cast alloys are composed of Mm-rich main phase (shallow black regions) and Ni-rich main phase (white gray regions) as well as a trace of Ce_2Ni_7 phase (small white regions). The morphologies and distributions of Mm-rich and Ni-rich phase vary with the increase of the amount of substituting Co with Fe. It displays that the concentration distribution of Mm-rich phase is changed into dispersion distribution with the increase of the amount of substituting Co with Fe. The reason for the presence of Ce_2Ni_7 phase is that the composition of the alloys is non-stoichiometric. It can be seen from Fig. 2 that the amount of the Ce_2Ni_7 phase decreases gradually with the increase of the Fe content. This is in agreement with the results analyzed by XRD.

Table 1
Lattice constants and cell volumes of the main phase in the as-cast and quenched alloys

Alloys	Lattice constants				Cell volume	
	a (Å)		c (Å)		V (Å)^3	
	As-cast	22 m/s	As-cast	22 m/s	As-cast	22 m/s
Fe_0	4.991	4.988	4.053	4.058	87.41	87.42
Fe_1	4.995	5.005	4.063	4.058	87.78	88.04
Fe_2	5.006	4.994	4.064	4.061	88.19	87.72
Fe_3	4.998	5.042	4.089	4.057	88.45	88.35
Fe_4	5.013	5.019	4.075	4.071	88.65	88.79
Fe_5	5.026	5.021	4.078	4.072	89.19	88.89
Fe_6	5.020	5.020	4.084	4.067	89.11	88.75

The longitudinal section morphologies of the as-quenched alloys with a quenching rate of 22 m/s were observed by SEM and the results were illustrated in Fig. 3. The grain of the as-quenched alloys is markedly refined with the increase of the Fe content although the same rapid quenching technology is used. The mechanism of substituting Co with Fe refining grains of the as-quenched alloys needs to be investigated further. The microstructure morphologies of the as-quenched alloys were observed by TEM and crystalline states of the as-quenched alloys were determined with SAD. The results were illustrated in Fig. 4. Fig. 4 shows the as-quenched Fe_0 and Fe_4 alloys have microcrystalline structures. The effect of substituting Co with Fe on crystalline state of the as-quenched alloys is almost imperceptible. The as-quenched Fe_0 and Fe_4 alloys with quenching rate of 22 m/s have an obvious tendency to form amorphous phase.

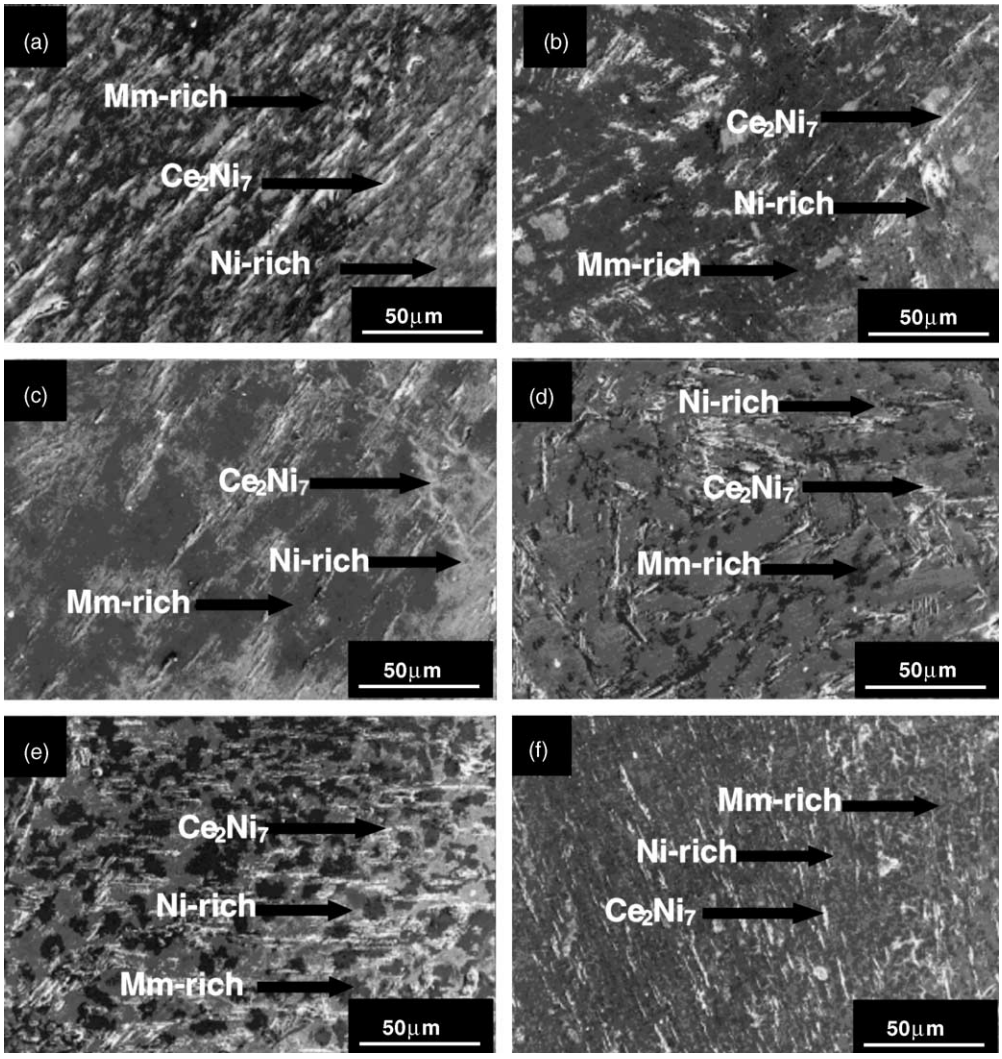

Fig. 2. The morphologies of the as-cast alloys (SEM) (a) Fe_0, (b) Fe_1, (c) Fe_2, (d) Fe_4, (e) Fe_5, and (f) Fe_6.

3.2. Electrochemical characteristics

3.2.1. Activation performance

The activation capability is characterized by the initial activation number. This initial activation number denoted by *n* is defined by the number of charge–discharge cycles required for attaining the maximum discharge capacity through a charge–discharge cycle at a constant current density. The cycle number dependence of the discharge capacities of the as-cast and quenched alloys is illustrated in Fig. 5, the charge–discharge current density being 60 mA/g. All of the as-cast and quenched alloys have an excellent activation performance. The as-cast and quenched alloys can be completely activated through two to four charge–discharge cycles. The

Table 2
The compositions of the main phases of the as-cast alloys (at.%)

Alloys	Main phases	Mm	Ni	Mn	Al	Si	Co	Fe	Fe/Co
Fe_0	Rich Mm	17.93	56.55	7.13	4.17	1.98	12.21	0	–
	Rich Ni	15.38	67.73	5.26	1.94	0.86	8.54	0	–
Fe_2	Rich Mm	17.25	57.32	6.95	3.98	2.01	8.31	4.17	0.50
	Rich Ni	15.02	68.12	5.31	2.28	0.87	5.38	2.94	0.55
Fe_4	Rich Mm	17.31	56.31	7.52	3.74	2.01	4.57	8.44	1.85
	Rich Ni	14.97	69.04	4.18	2.13	1.02	2.91	5.66	1.94
Fe_6	Rich Mm	17.58	55.83	8.46	3.68	2.13	0	12.24	–
	Rich Ni	14.71	70.12	40.60	2.73	0.91	0	7.44	–

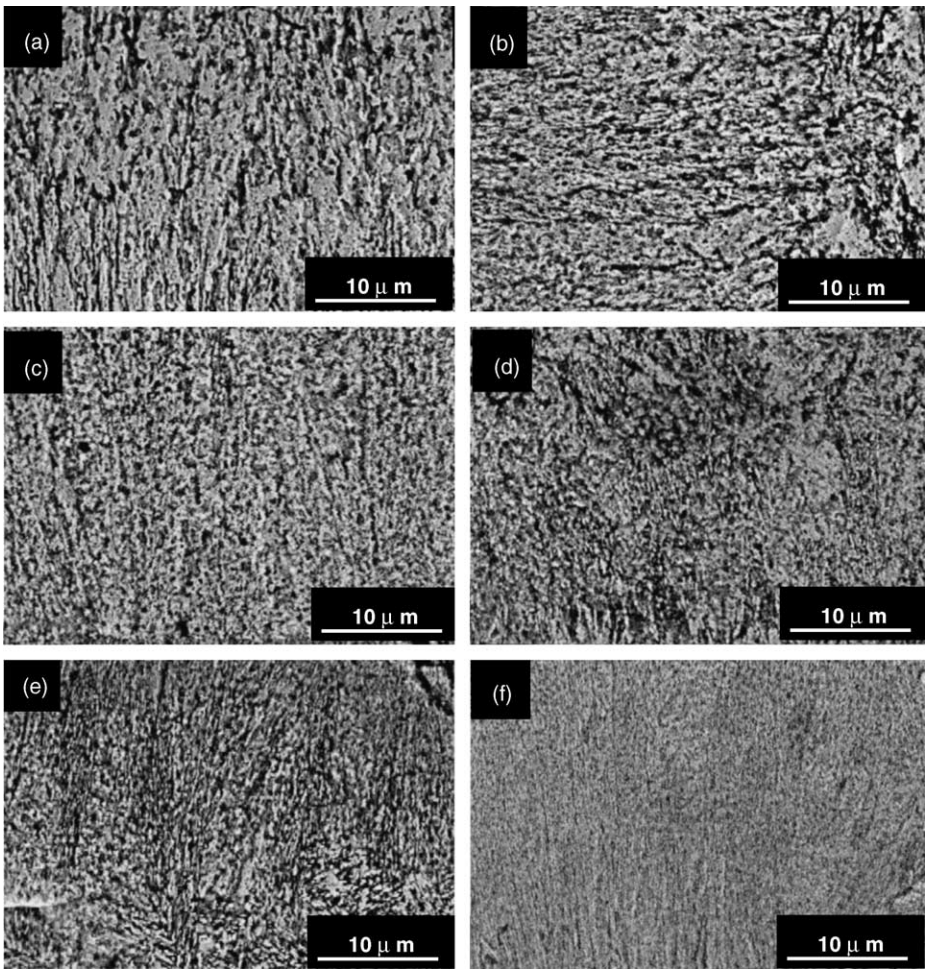

Fig. 3. Longitudinal section morphologies of the as-quenched (22 m/s) alloys taken by SEM (a) Fe_0, (b) Fe_1, (c) Fe_2, (d) Fe_3, (e) Fe_4, and (f) Fe_6.

substituting Co with Fe has a slight influence on the activation capability of the as-cast alloys. Generally, the activation capability of the hydrogen storage alloy is directly relevant to the change of the internal energy of the system before and after absorbing hydrogen. The larger the additive internal energy, which originates from oxidation film formed on the surface of the electrode alloy, and the strain energy, which is produced by hydrogen atom entering the interstitial of the tetrahedron or octahedron of the alloy lattice, the poorer is the activation performance of the alloy [11]. Obviously, decisive factors of the activation capability of the alloy are the phase structure, surface characteristic, grain size and interstitial dimensions of the alloy [12]. Substituting Co with Fe improves slightly activation performances of the as-quenched alloys. This is mainly attributed to the grain refinement of the as-quenched alloys produced by substituting Co with Fe. The increase of the lattice stress is inevitable when hydrogen atoms enter into the interstitials of the cell. The grain refinement increases grain boundary area. The grain boundary probably is a buffer area of the releasing of the lattice stress and strain energy, and enhances activation performances of the alloys.

3.2.2. Discharge capacity

The maximum discharge capacities of the as-cast and quenched alloys were measured with charge–discharge current density of 60 and 300 mA/g, respectively. The amount of substituting Co with Fe dependence of discharge capacities of the as-cast and quenched alloys is illustrated in Fig. 6. It can be seen from Fig. 6 that the discharge capacities of the as-cast and quenched alloys decrease with the increase of Fe content. When the Fe content x increases from 0 to 0.6, the maximum discharge capacities of the as-cast alloys decrease from 300.33 to 273.45 mAh/g and the maximum discharge capacities of the as-quenched alloys with quenching rate of 16 m/s decrease from 303.77 to 231.71 mAh/g. Obviously, the influence of substituting Co with Fe on the capacity of the as-quenched alloy is more significant than on that of the as-cast alloy. It can also be seen from Fig. 6 that the capacities of the as-quenched alloys, when the Fe content $x \leq 0.2$, decrease slightly with the increase of the Fe content. Contrarily, the capacities of the as-quenched alloys decrease greatly with the increase of the Fe content. It is probably attributed to the increase of the lattice stress of the as-quenched alloys produced by substituting Co with Fe.

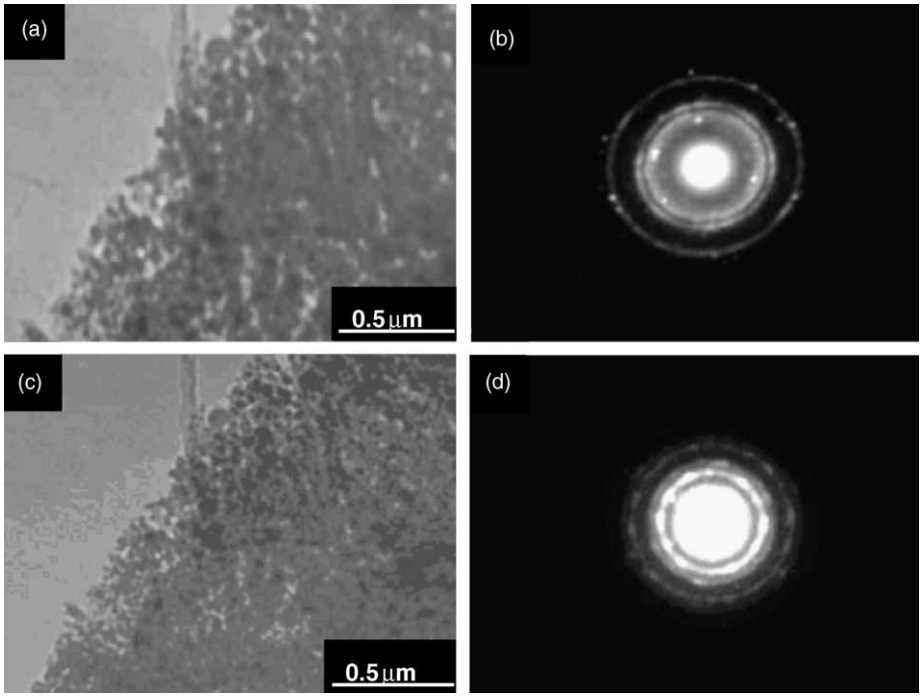

Fig. 4. The morphologies and SAD of the as-quenched (22 m/s) alloys taken by TEM (a) (b) morphology and SAD of Fe_0 alloy, (c) (d) morphology and SAD of Fe_4 alloy.

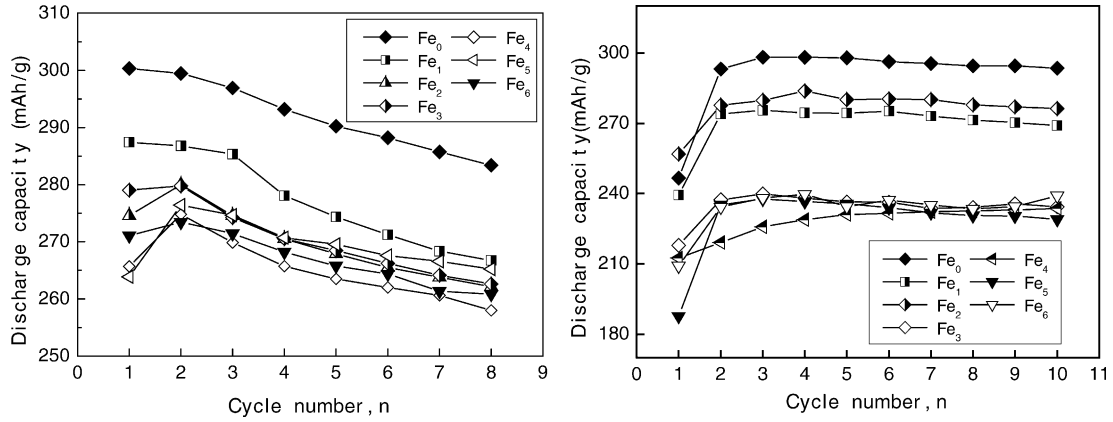

Fig. 5. The relationship between the cycle number and the discharge capacity of the alloys (a) as-cast and (b) as-quenched (22 m/s).

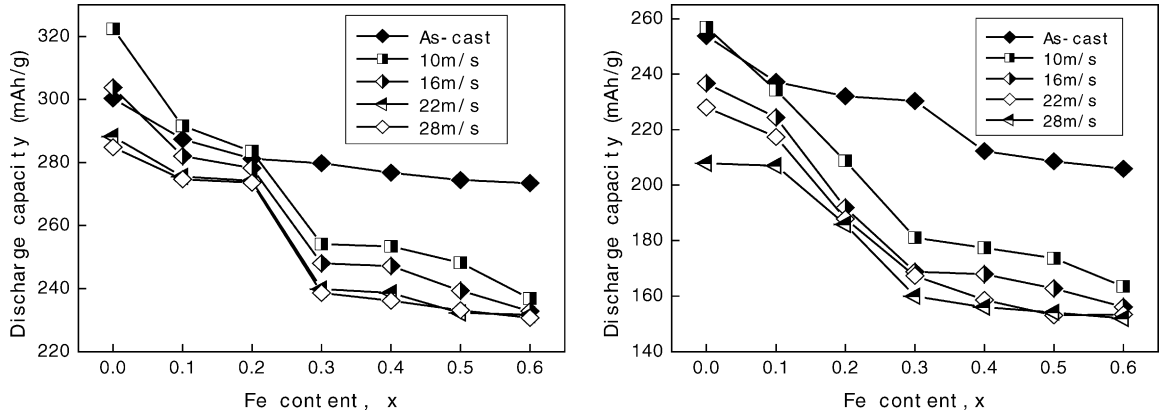

Fig. 6. The relationship between the Fe content and the discharge capacity of the alloys (a) 60 mA/g and (b) 300 mA/g.

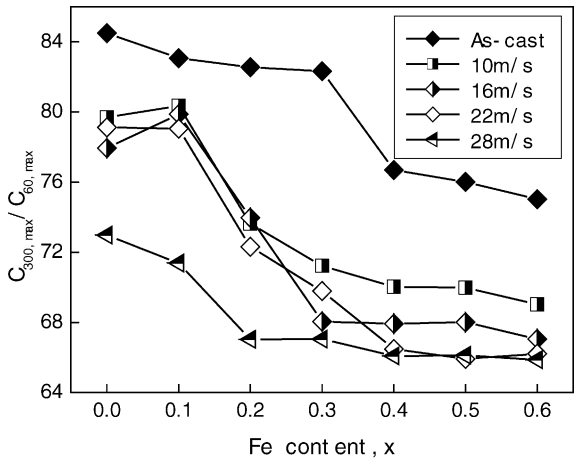

Fig. 7. The relationship between the Fe content and high rate discharge ability.

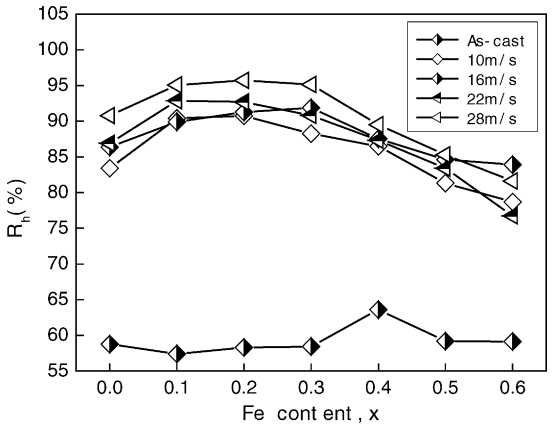

Fig. 8. The relationship between Fe content and capacity retaining rate (R_h).

3.2.3. High rate discharge ability (HRD)

Fig. 7 shows the relationship between the Fe content and 1C rate discharge abilities of the as-cast and quenched alloys. It can be seen from Fig. 7 that the rate discharge abilities of the alloys decrease with the increase of the Fe content. When Fe content increases from 0 to 0.6, the rate discharge abilities of the as-cast alloys decrease from 84.49 to 75.02% and that of the as-quenched alloys with quenching rate of 10 m/s decreases from 79.69 to 69.03%. The rate discharge ability is a dynamical problem of alloy electrode discharging. All factors, which decrease the diffusion capability of hydrogen atoms, decrease the high rate discharge ability of the alloys. Fe decreases the diffusion capability of hydrogen atoms in the alloys and increases the activation energy of hydrogen atom diffusion [13]. This is the main reason why substituting Co with Fe leads to the decrease of the high rate discharge abilities of the as-cast alloys.

3.2.4. Cycle life

In order to appraise accurately the cycle stability of the alloys, two definitions, capacity retaining rate and capacity decay rate, are introduced. The capacity retaining rate denoted by R_h is defined as $R_h = \frac{C_{300,300}}{C_{300,max}} \times 100\%$, where $C_{300,max}$ is the maximum discharge capacity when charge–discharge current density is 300 mA/g, and $C_{300,300}$ is the discharge capacity at 300th cycles, respectively. The capacity decay rate denoted by D is defined as $D = \frac{C_{300,max} - C_{300,300}}{300-n} \times 100\%$, where n is activation number. According to the above mentioned definitions, it can be known that the larger the capacity retaining rate (R_h), the smaller the capacity decay rate (D), and the better the cycle stability of the alloy. The Fe content dependence of the capacity retaining rates and the capacity decay rates of the as-cast and quenched alloys is illustrated in Fig. 8 and Fig. 9. Fig. 8 indicates that substituting Co with Fe can enhance capacity retaining rates of the as-cast alloys slightly and a maximum R_h of the as-quenched alloy can be obtained with the variety of Fe content. The effect of substituting Fe with Co on the cycle stability of the as-quenched alloys includes two favourable and unfavourable aspects. The grain refinement and the increase of the cell volume resulted from substituting Fe with Co is favourable, but the decrease of anti-corrosion ability produced by substituting Fe with Co is unfavourable. Therefore, it is certain that the capacity retaining rate R_h of the as-quenched alloy has a maximum value with the variety of the amount of substituting Fe with Co.

The cycle stability of the electrode alloy is an overwhelming factor of the life of Ni-MH battery. The root cause of leading to the efficacy loss of battery is on negative electrode rather than on positive electrode. The reason for substituting Co with Fe enhancing the cycle life of the as-cast alloys is mainly attributed to substituting Co with Fe leading to homogeneous distribution of Mm-rich main phase. Obviously, the uniformity of structure and composition can enhance the cycle stability of the alloy. The main cause of substituting Co with Fe enhancing the cycle stability of the as-quenched alloy is the grain refinement caused by substituting Co with Fe. The determining factors of the cycle life of the alloy are its anti-pulverization and oxidation capabilities. The smaller the grain size of the alloy, the stronger the strength and toughness, and the higher the anti-pulverization capability.

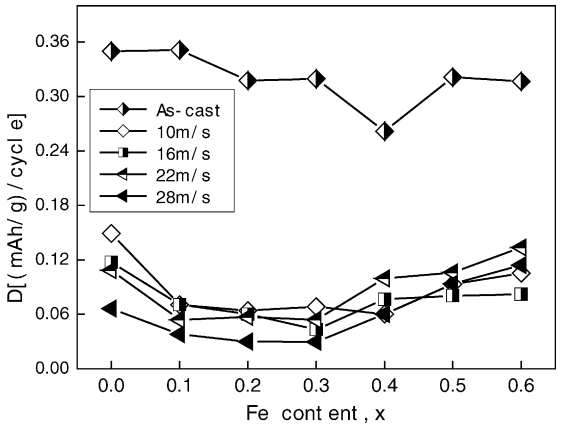

Fig. 9. The relationship between Fe content and capacity decay rate (D).

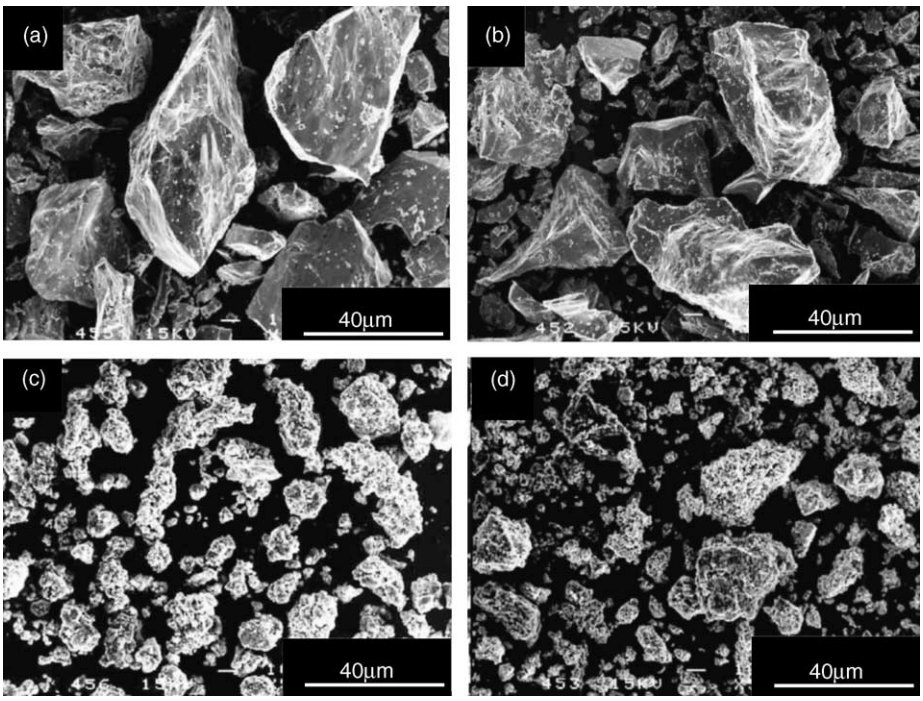

Fig. 10. The granular morphologies of as-cast alloys before and after electrochemical cycle (SEM) (a) Fe_0 before cycle, (b) Fe_4 before cycle, (c) Fe_0 after cycle, and (d) Fe_4 after cycle.

The morphologies of the as-cast Fe_0 and Fe_4 alloy particles before and after electrochemical cycle taken by SEM were shown in Fig. 10. Fig. 10 shows that the shapes of the alloy particles before electrochemical cycle are irregular and sharp-angled. This is characteristic of mechanical pulverization. After the as-cast Fe_0 and Fe_4 alloys passed 245 and 364 charge–discharge cycles, respectively, the morphologies of alloy particles changed markedly, leading to the disappearance of the pointedness of the particles and to the decrease of the particle sizes. This indicates that the main reason of leading to the capacity decay is the pulverization of the alloy. Worthy of remark is that cycle number of the as-cast Fe_4 alloy is 119 cycles larger than that of the as-cast Fe_0 alloy, whereas the particle sizes of the Fe_4 alloy are still larger than those of the Fe_0 alloy. Therefore, it can be concluded that anti-pulverization capability of the as-cast alloy can be improved by substituting Co with Fe. It can be seen from the particle morphologies after electrochemical cycle that the corrosion and oxidation of the surface of the alloy particles are trifling. This indicates that the main cause of leading to the efficacy loss of the electrode alloy is its pulverization during charge–discharge cycle.

4. Conclusion

1. The as-cast $Mm(NiMnSiAl)_{4.3}Co_{0.6-x}Fe_x$ ($x = 0$, 0.1, 0.2, 0.3, 0.4, 0.5, and 0.6) hydrogen storage alloys have a two-phase structure composed of a $CaCu_5$-type main phase and a small amount of Ce_2Ni_7 secondary phase. The amount of the secondary phase decreases after rapid quenching treatment with different quenching rate. The lattice constants and cell volumes of the as-cast and quenched alloys slightly increase with the increase of Fe content.
2. Substituting Co with Fe leads to the decrease of the discharge capacity of the alloy. The effects of Fe content on the capacities of the as-cast and quenched alloys are different. When Fe content increases from 0 to 0.6, the capacity of the as-cast alloy slightly decreases with the increase of Fe content. For the as-quenched alloys, when the Fe content $x \leq 0.2$, the capacities of the alloys decrease slightly with the increase of the Fe content. Contrarily, the capacities of the as-quenched alloys decrease greatly with the increase of the Fe content.
3. The cycle stabilities of the as-cast and quenched alloys are significantly improved by substituting Co with Fe. Especially, substituting Co with Fe can greatly enhance the cycle life of the as-quenched alloys when Fe content ≤ 0.3. It is because the grain of the as-quenched alloys can be markedly refined by substituting Co with Fe, which enhance anti-pulverization capability of the alloy in process of absorbing and desorbing hydrogen. When Fe content is more than 0.3, substituting Co with Fe leads to the decrease of the cycle stabilities of the as-quenched alloys. It probably is because substituting Co with Fe decreases the anti-corrosion abilities of the alloys.

Acknowledgement

This work is supported by National Natural Science Foundations of China (50131040 and 50071050).

References

[1] P. Li, X.-l. Wang, Y.-h. Zhang, R. Li, J.-m. Wu, X.-h. Qu, J. Alloys Compd. 353 (2003) 278.
[2] P. Li, X.-l. Wang, Y.-h. Zhang, J.-m. Wu, R. Li, X.-h. Qu, J. Alloys Compd. 352 (2003) 310.
[3] P. Li, Y.-h. Zhang, X.-l. Wang, Y.-f. Lin, X.-h. Qu, J. Power Sources 124 (2003) 285.
[4] J.M. Cocciantelli, P. Bernard, S. Fernandez, J. Atkin, J. Alloys Comp. 253–254 (1997) 642.
[5] W.-K. Hu, J. Alloys Comp. 279 (1998) 295.
[6] W.-K. Hu, D.-M. Kim, K.-J. Jang, J.-Y. Lee, J. Alloys Comp. 269 (1998) 254.
[7] W.-K. Hu, H. Lee, D.-M. Kim, S.-W. Jeon, J.-Y. Lee, J. Alloys Comp. 268 (1998) 261.
[8] W.-K. Hu, J. Alloys Comp. 289 (1999) 299.
[9] L. Jiang, F. Zhan, D. Bao, G. Qing, Y. Li, X. Wei, J. Alloys Comp. 231 (1995) 635.
[10] D. Chartouni, F. Meli, A. Züttel, K. Gross, L. Schlapbach, J. Alloys Comp. 241 (1996) 160.
[11] M.-S. Wu, H.-R. Wu, Y.-Y. Wang, C.-C. Wan, J. Alloys Comp. 302 (2000) 248.
[12] Y. Zhou, Y.-q. Lei, Y.-c. Luo, S.-a. Cheng, Q.-d. Wang, J. Acta Metallurgaca Sinica 32 (8) (1996) 857.
[13] C. Khaldi, H. Mathlouthi, J. Lamloumi, A. Percheron-Guégan, J. Alloys Comp. 360 (2003) 266.